10-27-2020

Delineating Heme-Mediated versus Direct Protein Oxidation in Peroxidase-Activated Cytochrome

Victor Yin

Derek Holzscherer

Lars Konermann

Delineating Heme-Mediated versus Direct Protein Oxidation in Peroxidase-Activated Cytochrome *c* by Top-Down Mass Spectrometry

Victor Yin, Derek Holzscherer, and Lars Konermann*

Department of Chemistry, The University of Western Ontario, London, Ontario, N6A 5B7, Canada

* corresponding author

E-mail address of the corresponding author: konerman@uwo.ca

Funding was provided by the Natural Sciences and Engineering Research Council of Canada (RGPIN-2018-04243).

Abbreviations: CID, collision induced dissociation; CT, chloramine-T; CT-holo-cyt *c*, CT-oxidized holo-cyt *c*; CT-aposs-cyt *c*, CT-oxidized apo-cyt *c* where Cys14 and Cys17 are linked by a disulfide bond; cyt *c*, cytochrome *c*; DTT, dithiothreitol; ESI, electrospray ionization; IM, ion mobility; GRT, Girard's reagent T; LysCHO, carbonylated lysine (aminoadipic semialdehyde); MetO, methionine sulfoxide; MP11, microperoxidase-11; MS, mass spectrometry; ROS, reactive oxygen species.

ABSTRACT: Oxidation of key residues in cytochrome *c* (cyt *c*) by chloramine T (CT) converts the protein from an electron transporter to a peroxidase. This peroxidase-activated state represents an important model system for exploring the early steps of apoptosis. CT-induced transformations include oxidation of the distal heme ligand Met80 (MetO, +16 Da), as well as carbonylation (LysCHO, -1 Da) in the range of Lys53/55/72/73. Remarkably, the 15 remaining Lys in cyt *c* are not susceptible to carbonylation. The cause of this unusual selectivity is unknown. Here we applied top-down mass spectrometry (MS) to examine whether CT-induced oxidation is catalyzed by heme. To this end, we compared the behavior of cyt *c* with (holo-cyt *c*) and without heme (aposs-cyt *c*). CT caused MetO formation at Met80 for both holo- and aposs-cyt *c*, implying that this transformation can proceed independently of heme. The aldehyde-specific label Girard's reagent T (GRT) reacted with oxidized holo-cyt *c*, consistent with the presence of several LysCHO. In contrast, oxidized apo-cyt *c* did not react with GRT, revealing that LysCHO only forms in presence of heme. The heme dependence of LysCHO formation was further confirmed using microperoxidase-11 (MP11). CT exposure of aposs-cyt *c* in the presence of MP11 caused extensive non-selective LysCHO formation. Our results imply that the selectivity of LysCHO formation at Lys53/55/72/73 in holo-cyt *c* is caused by the spatial proximity of these sites to the reactive (distal) heme face. Overall, this work highlights the utility of top-down MS for unravelling complex oxidative modifications.

Introduction

Covalent protein modifications by reactive oxygen species (ROS) impact numerous biological functions.[1-6] The presence of ROS is an unavoidable consequence of aerobic cellular respiration.[7] Oxidative modifications have been implicated in aging and neurodegenerative pathologies,[6, 8-10] Protein oxidation is also involved in sensing and signaling,[11-13] and it plays a major role for the efficacy and the shelf life of protein therapeutics.[14-16] Most protein oxidation events culminate in oxygen incorporation into side chains, e.g., Met → MetO (sulfoxide formation, +16 Da) or Lys-CH_2-NH_2 → Lys-CHO ("carbonylation", -1 Da). Many other pathways exist, and most residues can form various products (e.g., -2, +4, +16, +32, or +48 Da for Trp).[17-21]

In addition to oxidative modifications that occur within living cells, ROS can induce protein oxidation *in vitro*. Experimental strategies have been developed that use this approach for monitoring the solvent accessibility of individual side chains.[20-26] *In vitro* oxidative modifications also provide the opportunity to investigate oxidation-induced changes in protein structure, dynamics, and function.[5, 13, 24, 27-30]

Regardless of context (i.e., in living cells or in the test tube), many aspects of protein oxidation are complex and incompletely understood. For example, side chain oxidation by $^{\bullet}OH$ can be a relatively simple process that starts with addition to a double bond or hydrogen abstraction, followed by quenching of the protein radical by oxygen-containing species.[22] However, $^{\bullet}OH$ can also act via mechanisms that are more convoluted, by producing secondary oxidants which then attack the protein.[3, 5, 31, 32]

Some protein oxidation events are catalyzed by transition metals.[18, 33] Fenton-like reactions take place in the presence of peroxides, such as Fe(II) + H_2O_2 → Fe(III) + $^{\bullet}OH$ + OH^-. Subsequent metal reduction regenerates Fe(II) such that the process can continue, generating a steady supply

of •OH that attack the protein.[20, 22, 33] The peroxidase activity of some heme proteins represents another metal-catalyzed process.[34-36] In this case H_2O_2 reacts with Fe(III) heme to form "Compound I", a Fe(IV)=O species with an adjacent radical. Hydrogen abstraction from R-H sites then regenerates Fe(III).[37] The R• produced in this way undergo additional transformations which yield the final oxidation products. The aforementioned R-H can either be exogenous substrates or side chains in the vicinity of the heme; the latter scenario results in protein self-oxidation.[5, 38-41]

Many protein oxidation studies have focused on H_2O_2 and •OH,[20, 22] while other common oxidants have received less attention.[2, 42-44] Particular knowledge gaps persist for the widely used "mild" oxidant chloramine-T (CT, Figure S1).[29, 30, 43-48] In aqueous solution CT transforms into other reactive species that include OCl^-.[44, 46] The latter can cause side chain oxidation (e.g., Met + $OCl^- \rightarrow$ MetO + Cl^-), but alternative CT-induced protein oxidation pathways appear to exist.[46] The exact nature of these pathways remains to be explored.

Oxidative modifications of cytochrome *c* (cyt *c*, Figure 1) have attracted major attention over the past few years.[24, 29, 30, 41, 44, 47, 49-53] Cyt *c* acts as an electron transporter in the respiratory chain by cycling between its Fe(II)/(III) heme oxidation states.[54] In addition, cyt *c* can act as peroxidase that catalyzes the oxidation of cardiolipin in mitochondria, a key step during apoptosis.[53, 55-58] Interestingly, the peroxidase activity of native cyt *c* is very low because the heme iron is fenced in by a 6-coordinate environment, being ligated by four pyrrole nitrogens, His18, and Met80. To become an active peroxidase cyt *c* must undergo a structural transition that severs the Fe-Met80 bond and generates 5-coordinate heme with an open distal site. This 5-coordinate form is catalytically active because it allows for Fe-peroxide interactions with subsequent formation of reactive Fe(IV)=O species.[34, 36, 59] This peroxidase activation can be achieved by oxidative modifications of cyt *c*.[27, 29, 44, 47, 52] The most common *in vitro* activation method is cyt *c*

exposure to CT. The "CT-holo-cyt *c*" generated in this way has become a widely used model system for apoptosis research.[29, 30, 44, 47] For clarity, it is noted that CT is not encountered in living cells, where cyt *c* instead can be activated by other means such as H_2O_2 exposure and/or cardiolipin binding.[28, 41, 53]

We recently conducted a detailed mass spectrometry (MS)-based characterization of CT-holo-cyt *c*, and we found it to be a mixture of structurally and functionally diverse proteoforms.[27] In addition to MetO modifications at residues 80 and 65,[29, 44, 47, 52] CT-holo-cyt *c* carries up to three carbonylated Lys. Both Met80 oxidation and Lys carbonylation are essential for peroxidase activation. The former ruptures the Fe-Met80 bond and generates the vacant coordination site required for catalysis, while the latter ensures that this site remains vacant by preventing Fe-Lys coordination.[27] The presence of LysCHO in CT-holo-cyt *c* and in other oxidation-activated forms of the protein had long been overlooked[27, 28] but is now well accepted.[24, 41] A key finding of our previous work[27] was that despite cyt *c* possessing 19 Lys that are equally solvent-accessible,[60] only a small Lys cluster (53/55/72/73) was susceptible to LysCHO formation (Figure 1). The factors responsible for this unexpected specificity remain unexplored.

Here we tackle the mechanism by which CT induces oxidative modifications in cyt *c*. Specifically, we investigated whether these transformations are mediated by the heme cofactor, keeping in mind the role of transition metal centers during the oxidation of other proteins.[20, 22, 33] The strategy of our experiments is simple - we compared the effects of CT on holo-cyt *c* and apo-cyt *c* (the heme-free variant of the protein). Our work applied various MS tools. A particularly powerful approach is the fragmentation of intact proteins by top-down MS/MS via collision-induced dissociation (CID), followed by ion mobility (IM) separation and mass analysis of fragment ions. This top-down CID-IM-MS method[61-63] is superior to traditional bottom-up MS in

cases where protein modifications such as LysCHO interfere with tryptic digestion, peptide ionization and fragmentation.[27] Our experiments uncovered that Met → MetO conversion in cyt *c* can proceed in a heme-independent fashion. In contrast, LysCHO formation requires heme catalysis, a finding that explains the spatial selectivity of Lys carbonylation.

Methods

Materials. Equine cyt *c,* CT, dithiothreitol (DTT), Girard's reagent T (GRT, (carboxymethyl)trimethylammonium chloride hydrazide), Tris base (2-amino-2-(hydroxymethyl)-1,3-propanediol), guanidinium chloride, and AgCl were supplied by MilliporeSigma (St. Louis, MO). Acetonitrile and ammonium acetate were from Fisher (Nepean, ON). Potassium phosphate was from Caledon (Georgetown, ON). MS-grade modified trypsin was obtained from Promega (Madison, WI). Centrifuge filters (Amicon Ultra 0.5, 10 kDa MWCO) were supplied by Millipore Sigma, and used following manufacturer instructions (15 min at 13,000 G; buffer exchange steps were performed using four cycles). Unless stated otherwise, reactions were performed at 22 ± 2 °C, and solutions contained 50 mM potassium phosphate (pH 7.4).

Mass Spectrometry. Electrospray MS experiments were conducted on a Waters SYNAPT G2-Si Q-ToF in positive ion mode. MS/MS was performed using CID with Ar as collision gas. Samples were prepared as 5 μM protein solutions in 50/50/0.1% H_2O/acetonitrile/formic acid that were infused directly into the electrospray ionization (ESI) source of instrument at 5 μL min^{-1}. Top-down CID-IM-MS was performed as described.[27] Briefly, quadrupole-selected 16+ cyt *c* ions corresponding to the proteoforms of interest were collisionally heated in Ar background gas in the

trap cell. Trap collision energies were adjusted between 22 and 25 V to maximize the fragment ion yield and sequence coverage. The resulting fragment ions were separated in the traveling-wave IMS cell with N_2 as buffer gas, followed by reflectron-time-of flight mass analysis. Bottom-up samples were digested overnight at 37 °C using a 50:1 protein:trypsin ratio. Tryptic peptides were separated on a Waters ACQUITY UPLC BEH C18 column (1.7 μm, 2.1 × 10 mm) with a H_2O/acetonitrile gradient in the presence of 0.1% formic acid. MS/MS data were collected using data-dependent acquisition. Isotope distributions were modeled following strategies developed previously[64] using Protein Prospector (http://prospector.ucsf.edu), with N-terminal acetylation, and with heme in the Fe(III) oxidation state. For example, 16+ holo-cyt *c* was modeled with 15 excess protons, keeping in mind that Fe(III) heme (with both propionic acid groups in the R-COOH state) has an overall charge of 1+.[65] Using this approach, the deconvoluted average mass of holo-cyt *c* is calculated to be 12360.1833 Da, in agreement with previous work.[44] MetO and LysCHO formation events corresponds to mass shifts of +15.9949 Da and -1.0316 Da, respectively.[18]

Heme Removal: Preparation of apo$_{SS}$-cyt *c*. Heme in cyt *c* is covalently bound by thioether linkages to Cys14 and Cys17.[60] Heme removal was performed as described[66] with some modifications. Cys-S-heme bonds were initially replaced with Cys-S-Ag bonds. For this purpose, 200 μL glacial acetic acid were added to 1.8 mL of an aqueous solution of 400 μM cyt *c* and 25 mM AgCl, followed by incubation at 40 °C in the dark for 4 h and centrifugation at 13,000 G for 5 min. The supernatant was buffer exchanged into 100 mM acetic acid, yielding apo-cyt *c* carrying up to three silver ions (Ag-apo-cyt *c*, Figure 2B). For Ag removal, 100 μL Ag-apo-cyt *c* were added to 900 μL of 50 mM pH 5 ammonium acetate containing 6 M guanidinium chloride and 1 M DTT, followed by incubation for 3 h. Samples were then buffer exchanged into 50 mM pH 5

ammonium acetate, yielding apo-cyt *c* (ε_{280} = 10.9 mM^{-1} cm^{-1})[67] with both Cys14 and Cys17 in the thiol form. The absence of heme was confirmed by MS (Figure 2C) and UV-Vis (Figure S2). The apo-cyt *c* generated in this way underwent a mass shift of -2 Da during storage (Figure 3A) that was reversible by DTT (Figure S3), indicating -SS- bond formation between Cys14 and Cys17. To obtain homogeneous stable heme-free samples we promoted formation of this -SS- bond by storing 10 μM apo-cyt *c* for 24 h at 22 °C, followed by overnight incubation at 4 °C. The disulfide-containing protein generated in this way is referred to apoSS-cyt *c*. Top-down CID-IM-MS confirmed the presence of a disulfide between Cys14 and Cys17 in apoSS-cyt *c*, while also verifying the absence of other covalent modifications (Figure 3B, C).

CT-induced Oxidation and GRT Labeling. 50 μM apoSS-cyt *c* or holo-cyt *c* were incubated in 2.5 mM CT/50 mM pH 8.4 Tris buffer for 3 h.[68, 69] The reaction was halted by buffer exchange into 50 mM pH 5 ammonium acetate, yielding CT-apoSS-cyt *c* and CT-holo-cyt *c*. We also prepared apoSS-cyt *c* samples that were less extensively oxidized by using 0.5 mM instead of 2.5 mM CT (CT_{low}-apoSS-cyt *c*). Oxidation in the presence of microperoxidase 11 (MP11) was performed using the same procedures, except that 50 μM MP11 was added to the CT/protein mixture. Covalent tagging of reactive carbonyl groups was performed using GRT[15] by incubating 10 μM protein (CT-treated or unoxidized controls) with 80 mM GRT in 50 mM pH 5 ammonium acetate for 3 h. Excess GRT was removed by buffer exchange into 50 mM pH 5 ammonium acetate.

Results and Discussion

For probing the role of heme during CT-induced cyt *c* oxidation we compared the behavior of the native protein and its heme-free counterpart. To assist readers, we briefly recapitulate the sample types that were used here, and that were prepared as described above: (i) Holo-cyt *c* is the native protein, possessing a covalently attached heme. (ii) Aposs-cyt *c* is devoid of heme, and its Cys14 and Cys17 side chains are linked by a -SS- bond (Figure 3). (iii) CT-holo-cyt *c* refers to holo-cyt *c* after oxidation by CT, comprising various proteoforms with MetO formation at residues 80 and 65, and one or more LysCHO in the Lys53/55/72/73 range.[27] (iv) CT-aposs-cyt *c* refers to aposs-cyt *c* after oxidation by CT, under conditions identical to those used for CT-holo-cyt *c*. (v) CT_{low}-aposs-cyt *c* was exposed to a five-fold lower CT concentration than CT-aposs-cyt *c*. Oxidative modifications in CT-aposs-cyt *c* and CT_{low}-aposs-cyt *c* have not been characterized previously.

Effects of CT-Induced Oxidation. Intact protein mass spectra of the aforementioned protein species are depicted in Figure 4. CT-holo-cyt *c* and CT-aposs-cyt *c* both showed oxidative modifications, with ~16 Da peak progressions that represent the hallmark of +*n*O incorporation (Figure 4B, D, E). Similar patterns have previously been reported for other oxidized proteins.[5, 20, 22] Background oxidation for CT-free samples was negligible (Figure 4A, C). The spectrum of CT-holo-cyt *c* had its maximum at +2 O (Figure 4B), while that of CT-aposs-cyt *c* was dominated by signals around +4 O (Figure 4E). This observation reveals that heme removal renders cyt *c* more susceptible to oxidation by CT. Comparable oxidation levels to holo-cyt *c* could be achieved only when incubating aposs-cyt *c* samples in five-fold less CT (Figure 4D).

Close inspection of Figure 4 reveals deviations from "clean" +*n*O behavior. In CT-holo-cyt *c,* the signals were shifted by -2 Da due to LysCHO formation (Figure 4B).[27] CT-aposs-cyt *c* showed a similar negative shift (Figure 4E). This -2 Da shift was absent for CT_{low}-aposs-cyt *c*

(Figure 4D). While the -2 Da shift in Figure 4E seems to suggest the presence of LysCHO in CT-aposs-cyt *c*, the data discussed below reveal that it has a different origin.

It may seem counterintuitive that heme removal enhances the oxidation susceptibility of cyt *c*, considering the capability of metal centers to catalyze oxidation.[20, 22, 33-36] However, metal catalysis is not the only factor that is relevant in this context. CD spectroscopy revealed that heme removal causes cyt *c* unfolding (Figure S4), confirming earlier reports that the protein structural integrity is contingent on heme.[66] The enhanced oxidation susceptibility of aposs-cyt *c* is attributable to the fact that unfolding renders previously buried side chains sterically accessible to CT. This interpretation is in line with studies on other proteins where unfolding was found to enhance modifications by water-soluble labeling agents.[20, 22, 70, 71]

Oxidation Site Mapping. We performed top-down CID-IM-MS to identify the modifications in CT-aposs-cyt *c* and CT_{low}-aposs-cyt *c* (Figure 5). Data for CT-holo-cyt *c* were included for comparison (Figure S5), although an in-depth analysis of the latter has already been reported.[27] All top-down experiments were performed by fragmenting [M + "2 O"] ions. The quotation marks indicate the presence of additional -2 Da modifications in CT-holo- cyt *c* and CT-aposs-cyt *c* that cause deviations from "clean" +2 O (+32 Da) Da mass shifts. Fragment spectra of all three CT-oxidized forms shared a y_{24} to [y_{25} + O] transition, as well as a [y_{39} + O] to [y_{40} + 2 O] transition (Figures 5, S5). This pattern confirms MetO formation at both Met80 and Met65 for all three species (CT-holo-, CT-aposs-, and CT_{low}-aposs-cyt *c*). These observations demonstrate that CT-induced MetO formation can take place without heme catalysis. This conclusion is in line with the fact that Met is one of the most easily oxidizable residues,[20] that is known to be capable of forming MetO without metal catalysis.[45, 72, 73]

A more intriguing question is the nature of the -2 Da shift in CT-aposs-cyt *c* (Figure 4E). As noted, -2 Da shifts in CT-holo-cyt *c* are caused by LysCHO formation in the range of Lys53/55/72/73.[27] Does CT-aposs-cyt *c* contain these modifications as well? The top-down data of Figure 5 localize the -2 Da modification in CT-aposs-cyt *c* between residues 49 and 64, ruling out modifications at Lys72/73. The 49-64 range comprises Lys53/55/60 such that LysCHO formation could, in principle, be a possible explanation of the observed -2 Da shift. However, subsequent experiments demonstrated that CT-aposs-cyt *c* is free of LysCHO (see details below).

Confirming LysCHO Sites by GRT Labeling. GRT is a hydrazide compound that selectively reacts with ketones and aldehydes (such as LysCHO). Other modified side chains that might potentially be present (such as Tyr dimers, -2 Da)[5] do not react with GRT.[15, 74, 75] GRT labeling of CT-holo-cyt *c* produced satellite peaks corresponding to +1 GRT and +2 GRT, confirming the presence of two LysCHO sites that are responsible for the -2 Da mass shift of CT-holo-cyt *c* (Figure 6B).[27] Top-down CID-IM-MS of the most intense GRT adduct confirmed GRT labeling at Lys72/73 (Figure S6), in agreement with earlier work.[27]

Given the much higher overall oxidation propensity of CT-aposs-cyt *c* relative to CT-holo-cyt *c* (Figure 4), one might expect correspondingly more LysCHO sites (and thus more extensive GRT labeling). Surprisingly, CT-aposs-cyt *c* was completely unreactive with GRT (Figure 6D). The same was observed for CT_{low}-aposs-cyt *c* (Figure S7). This lack of GRT reactivity reveals that CT is incapable of forming LysCHO in aposs-cyt *c*. It can be concluded that LysCHO is not a general byproduct of CT-induced oxidation. Instead, Figure 6 strongly suggests that CT can induce LysCHO formation only in the presence of heme.

As LysCHO is absent in CT-apoSS-cyt *c,* the -2 Da shift in this protein form must arise from another modification. As noted earlier, top-down CID-IM-MS localized the -2 Da shift to ^{49}TDANKNKGITWKEETL^{64} (Figure 5). Scenarios such as ThrCH-OH → ThrC=O (-2 Da)[20, 21] can be excluded by the lack of GRT labeling in CT-apoSS-cyt *c*. Trp is the residue with the highest intrinsic oxidation propensity in the 49-64 range.[20] Studies on other proteins showed that Trp can yield various oxidation products, including -2 Da species.[76] Using bottom-up MS/MS we were able to detect low-level Trp59 oxidation in CT-apoSS-cyt *c* (Figure S8). Unfortunately, we could not unequivocally attribute the -2 Da mass shift to Trp59 in these experiments. Based on the arguments outlined above, Trp59 nonetheless represents the most likely culprit for the -2 Da modification in CT-apoSS-cyt *c*. The unfolded structure of apoSS-cyt *c* increases the reactivity of Trp59,[66] while in native holo-cyt *c* this residue is buried.[60] This enhanced solvent exposure renders Trp59 more prone to oxidation in apoSS-cyt *c*.[20, 22, 70, 71]

Confirming Heme Catalyzed LysCHO Formation Using MP11. The absence of LysCHO in CT-apoSS-cyt *c* strongly suggests that this type of modification can form only with heme catalysis. However, skeptics might point out that other differences between holo-cyt *c* and apoSS-cyt *c* could play a role as well. For example, it could be possible that the absence of LysCHO in CT-apoSS-cyt *c* is somehow related to the unfolded structure of this protein form (Figure S4). To conclusively test the role of heme, we produced CT-apoSS-cyt *c* in the presence of exogenous heme in the form of MP11. MP11 is a heme-containing cyt *c* fragment (residues 11-21). The Fe(III) in MP11 is coordinated by His18 while the distal site remains open, allowing MP11 to catalyze a range of oxidation reactions.[77, 78] The covalent thioether linkages in MP11 preclude reconstitution of native

holo-cyt *c* upon mixing with aposs-cyt *c*, allowing us to delineate the effects of protein conformation vs. heme involvement on protein oxidation.

The presence of MP11 during CT-aposs-cyt *c* formation profoundly impacted the mass spectra (Figure 7). The most obvious effect was a dramatic shift toward lower charge states (i.e. from maxima around 16+/17+ down to 11+/12+) which indicates the loss of numerous charge-bearing sites (i.e., Lys-CH_2-NH_3^+ → $LysCHO^0$).[79] Abundant LysCHO formation is also apparent from the mass distribution (Figure 7F) which shifted by ca. -10 Da, corresponding to ca. 10 LysCHO. We attempted to use GRT labeling of MP11/CT-aposs-cyt *c* for confirming the presence of LysCHO; however, those experiments yielded spectra with low S/N that were difficult to analyze (not shown). Keeping in mind that aposs-cyt *c* does not react with GRT due to the absence of LysCHO (Figures 6D, S7B), this low S/N likely arises from over-labeling of MP11/CT-aposs-cyt *c* by GRT. To nonetheless obtain direct confirmation of LysCHO, we performed MP11 experiments under the milder oxidation conditions of CT_{low}-aposs-cyt *c.* These experiments yielded the expected GRT-labeled products, confirming the ability of MP11 to induce the conversion of Lys to LysCHO (Figure S9B,C).

In summary, our data reveal that LysCHO formation by CT is a heme-dependent process. This finding explains the unusual selectivity of LysCHO formation in CT-holo-cyt *c* which affects only four out of 19 Lys.[27] All of the affected residues (Lys53/55/72/73) are in close spatial proximity to the reactive (distal) heme face,[27] rendering them poised for heme-catalyzed oxidation (Figure 1). It is possible that these oxidation events involve *direct* Lys-heme interactions, because rupture of the Met80-Fe bond facilitates structural changes that can trigger "alkaline" Lys-Fe ligation involving residues 53/55/72/73.[27, 30, 80-83] Lys residues other than 53/55/72/73 are not oxidized in holo-cyt *c* because they lack the spatial requirements for interaction with the

endogenous heme. This spatial selectivity is reminiscent of metal-catalyzed oxidation in other proteins.[33] In contrast, exposure of aposs-cyt *c* to freely diffusible heme (in the form of MP11) removes this geometric requirement, allowing heme to freely sample positions close to any of the 19 Lys and thus resulting in non-selective "global" LysCHO formation (Figure 7F). This non-selectivity is also apparent from the multiple fragment ion populations seen by top-down CID-IM-MS of GRT-labeled MP11/CT_{low}-aposs-cyt *c* (Figure S9D).

Conclusions

CT-holo-cyt *c* represents an important model system that mimics the state produced *in vivo* when cells embark on their path towards apoptosis.[27, 29, 30, 44, 47] CT-induced oxidation of cyt *c* produces a 5-coordinate Fe(III) that is required for peroxidase activity. These modifications were identified as MetO at residue 80, as well as LysCHO formation in the Lys53/55/72/73 range.[27] The current work provides new insights into the chemistry underlying these transformations. In agreement with previous reports[45, 72, 73] we found that CT-induced MetO formation can proceed without heme (although the direct Met80-heme contact in holo-cyt *c* may enhance the rate of oxidation at that residue). In contrast, CT-induced LysCHO formation strictly requires the presence of heme as a catalyst, and it only takes place in the direct vicinity of heme. The heme can be endogenous as in the case of holo-cyt *c*, or it can be exogenous as in our MP11 experiments.

The role of metal catalysis during CT-induced oxidation of small organic substrates has been examined previously, e.g. for Os(VIII) oxide and In(III) triflate.[46, 84] However, there seems to be no prior work related to the reactivity of CT in the presence of Fe or heme. We consider it most likely that the heme-catalyzed Lys oxidation seen here involves OCl^-. It is known that CT

produces OCl^-,[44, 46] and it is also known that OCl^- interacts with heme to generate Compound I and related Fe(IV)=O species.[85-87] The formation of such species in our MP11 experiments is favored by the fact that the distal heme face in MP11 is freely accessible.[77, 78] In the case of holo-cyt *c*, OCl^--Fe interactions require opening of the heme crevice. Such opening events are facilitated by the high flexibility of the 71-85 Ω loop that covers the distal heme face in native cyt *c*.[88, 89] Disruption of the Fe-Met80 contact via MetO formation further enhances the tendency of this Ω loop to sample oxidant-accessible conformation.[28, 90, 91]

It is tempting to speculate on the broader implications of heme-catalyzed LysCHO formation, relative to other oxidation pathways. Compound I-dependent oxidation involves the abstraction of H atoms by radical oxygen species.[34] Analogous H abstraction takes place during other oxidation methods, e.g. Fenton chemistry[33] or direct exposure to •OH.[20] Likely, all of these methods generate similar (if not identical) types of oxidation products. It is therefore surprising that LysCHO formation has been observed after Fenton reactions[92] and other metal-catalyzed processes,[18] but not after direct •OH exposure.[20, 21] One possible explanation is that LysCHO tends to go undetected in conventional bottom-up LC-MS/MS workflows because LysCHO sites interfere with tryptic digestion and collision-induced dissociation of peptides.[27] Future work is required to explore this issue in more detail.

From a bioanalytical perspective, this work demonstrates that top-down MS is highly suitable for interrogating heterogeneous oxidative modifications, including LysCHO sites which are difficult to track when using traditional bottom-up workflows.[27] Future top-down investigations will be aided by continuing advancements in instrumentation that enable high-resolution analyses of proteins with ever-increasing size and complexity.[93-95] It is hoped that this work will stimulate further top-down MS studies in the exciting field of protein oxidation.

Supporting Information. Structure of CT. UV/vis absorption spectra of cyt *c* before and after heme removal. Mass spectra of DTT-treated apoSS-cyt *c*. Far-UV CD spectra of cyt *c.* Top-down CID-IM-MS of CT-holo-cyt *c*. Top-down CID-IM-MS of GRT-labeled CT-holo-cyt *c*. Mass spectra of GRT-treated CT_{low}-apoSS-cyt *c*. Bottom-up MS/MS of oxidized Trp peptides. Mass spectra of GRT-labeled MP11/CT_{low}-apoSS-cyt *c*.

Accession Codes

Cytochrome *c* from *Equus caballus* (horse), UniProtKB P00004.

References

1. Berlett, B. S., and Stadtman, E. R. (1997) Protein oxidation in aging, disease, and oxidative stress, *J. Biol. Chem. 272*, 20313-20316.
2. Radi, R. (2018) Oxygen radicals, nitric oxide, and peroxynitrite: Redox pathways in molecular medicine, *Proc. Natl. Acad. Sci. U. S. A. 115*, 5839-5848.
3. Winkler, J. R., and Gray, H. B. (2015) Electron flow through biological molecules: does hole hopping protect proteins from oxidative damage?, *Q. Rev. Biophys. 48*, 411-420.
4. Nimse, S. B., and Pal, D. (2015) Free radicals, natural antioxidants, and their reaction mechanisms, *RSC Adv. 5*, 27986-28006.
5. Kathiresan, M., and English, A. M. (2017) LC-MS/MS suggests that hole hopping in cytochrome c peroxidase protects its heme from oxidative modification by excess H2O2, *Chem. Sci. 8*, 1152-1162.
6. Dalle-Donne, I., Rossi, R., Giustarini, D., Milzani, A., and Colombo, R. (2003) Protein carbonyl groups as biomarkers of oxidative stress, *Clin. Chim. Acta 329*, 23-38.
7. Gray, H. B., and Winkler, J. R. (2018) Living with Oxygen, *Accounts Chem. Res. 51*, 1850-1857.
8. de Graff, A. M. R., Hazoglou, M. J., and Dill, K. A. (2016) Highly Charged Proteins: The Achilles' Heel of Aging Proteomes, *Structure 24*, 329-336.
9. Pedersen, J. T., Chen, S. W., Borg, C. B., Ness, S., Bahl, J. M., Heegaard, N. H. H., Dobson, C. M., Hemmingsen, L., Cremades, N., and Teilum, K. (2016) Amyloid-beta and alpha-Synuclein Decrease the Level of Metal-Catalyzed Reactive Oxygen Species by Radical Scavenging and Redox Silencing, *J. Am. Chem. Soc. 138*, 3966-3969.
10. Sultana, R., Boyd-Kimball, D., Poon, H. F., Cai, J., Pierce, W. M., Klein, J. B., Markesbery, W. R., Zhou, X. Z., Lu, K. P., and Butterfield, D. A. (2006) Oxidative modification and down-regulation of Pin1 in Alzheimer's disease hippocampus: A redox proteomics analysis, *Neurobiol. Aging 27*, 918-925.
11. Giorgio, M., Trinei, M., Migliaccio, E., and Pelicci, P. G. (2007) Hydrogen peroxide: a metabolic by-product or a common mediator of ageing signals?, *Nat. Rev. Mol. Cell Biol. 8*, 722A-728.
12. Lee, J. W., and Helmann, J. D. (2006) The PerR transcription factor senses H2O2 by metal-catalysed histidine oxidation, *Nature 440*, 363-367.
13. Heppner, D. E., Dustin, C. M., Liao, C. Y., Hristova, M., Veith, C., Little, A. C., Ahlers, B. A., White, S. L., Deng, B., Lam, Y. W., Li, J. N., and van der Vliet, A. (2018) Direct cysteine sulfenylation drives activation of the Src kinase, *Nat. Commun. 9*, 1-11.
14. Beck, A., Wagner-Rousset, E., Ayoub, D., Van Dorsselaer, A., and Sanglier-Cianferani, S. (2013) Characterization of Therapeutic Antibodies and Related Products, *Anal. Chem. 85*, 715-736.
15. Yang, Y., Stella, C., Wang, W. R., Schoneich, C., and Gennaro, L. (2014) Characterization of Oxidative Carbonylation on Recombinant Monoclonal Antibodies, *Anal. Chem. 86*, 4799-4806.
16. Bobst, C. E., Thomas, J. J., Salinas, P. A., Savickas, P., and Kaltashov, I. A. (2010) Impact of oxidation on protein therapeutics: Conformational dynamics of intact and oxidized acid-beta-glucocerebrosidase at near-physiological pH, *Protein Sci. 19*, 2366-2378.
17. Madian, A. G., and Regnier, F. E. (2010) Proteomic Identification of Carbonylated Proteins and Their Oxidation Sites, *J. Proteome Res. 9*, 3766-3780.

18. Møller, I. M., Rogowska-Wrzesinska, A., and Rao, R. S. P. (2011) Protein carbonylation and metal-catalyzed protein oxidation in a cellular perspective, *J. Proteomics 74*, 2228-2242.
19. Yang, J., Wang, S., Liu, J., and Raghani, A. (2007) Determination of tryptophan oxidation of monoclonal antibody by reversed phase high performance liquid chromatography, *J. Chromatogr. A 1156*, 174-182.
20. Xu, G., and Chance, M. R. (2007) Hydroxyl Radical-Mediated Modification of Proteins as Probes for Structural Proteomics, *Chem. Rev. 107*, 3514-3543.
21. Johnson, D. T., Di Stefano, L. H., and Jones, L. M. (2019) Fast photochemical oxidation of proteins (FPOP): A powerful mass spectrometry-based structural proteomics tool, *J. Biol. Chem. 294*, 11969-11979.
22. Liu, X. R., Zhang, M. M., and Gross, M. L. (2020) Mass Spectrometry-Based Protein Footprinting for Higher-Order Structure Analysis: Fundamentals and Applications, *Chem. Rev. 120*, 4355−4454.
23. Li, X. Y., Grant, O. C., Ito, K., Wallace, A., Wang, S. X., Zhao, P., Wells, L., Lu, S., Woods, R. J., and Sharp, J. S. (2017) Structural Analysis of the Glycosylated Intact HIV-1 gp120-b12 Antibody Complex Using Hydroxyl Radical Protein Footprinting, *Biochemistry 56*, 957-970.
24. Chea, E. E., Deredge, D. J., and Jones, L. M. (2020) Insights on the Conformational Ensemble of Cyt C Reveal a Compact State during Peroxidase Activity, *Biophys. J. 118*, 128-137.
25. Calabrese, A. N., Ault, J. R., Radford, S. E., and Ashcroft, A. E. (2015) Using hydroxyl radical footprinting to explore the free energy landscape of protein folding, *Methods 89*, 38-44.
26. McClintock, C. S., Parks, J. M., Bern, M., GhattyVenkataKrishna, P. K., and Hettich, R. L. (2013) Comparative Informatics Analysis to Evaluate Site-Specific Protein Oxidation in Multidimensional LC-MS/MS Data, *J. Proteome Res. 12*, 3307-3316.
27. Yin, V., Mian, S. H., and Konermann, L. (2019) Lysine carbonylation is a previously unrecognized contributor to peroxidase activation of cytochrome c by chloramine-T, *Chem. Sci. 10*, 2349-2359.
28. Yin, V., Shaw, G. S., and Konermann, L. (2017) Cytochrome c as a Peroxidase: Activation of the Pre-Catalytic Native State by H2O2-Induced Covalent Modifications, *J. Am. Chem. Soc. 139*, 15701–15709.
29. Capdevila, D. A., Marmisolle, W. A., Tomasina, F., Demicheli, V., Portela, M., Radi, R., and Murgida, D. H. (2015) Specific methionine oxidation of cytochrome c in complexes with zwitterionic lipids by hydrogen peroxide: potential implications for apoptosis, *Chem. Sci. 6*, 705-713.
30. Zhong, F., and Pletneva, E. V. (2018) Ligation and Reactivity of Methionine-Oxidized Cytochrome c, *Inorg. Chem. 57*, 5754-5766.
31. Vahidi, S., and Konermann, L. (2016) Probing the Time Scale of FPOP (Fast Photochemical Oxidation of Proteins): Radical Reactions Extend Over Tens of Milliseconds, *J. Am. Soc. Mass Spectrom. 27*, 1156-1164.
32. Saladino, J., Liu, M., Live, D., and Sharp, J. S. (2009) Aliphatic Peptidyl Hydroperoxides as a Source of Secondary Oxidation in Hydroxyl Radical Protein Footprinting, *J. Am. Soc. Mass Spectrom. 20*, 1123-1126.

33. Bridgewater, J. D., Lim, J., and Vachet, R. W. (2006) Using Metal-Catalyzed Oxidation Reactions and Mass Spectrometry to Identify Amino Acid Residues Within 10 Å of the Metal in Cu-Binding Proteins, *J. Am. Soc. Mass Spectrom. 17*, 1552-1559.
34. Veitch, N. C. (2004) Horseradish peroxidase: a modern view of a classic enzyme, *Phytochem. 65*, 249-259.
35. Rodriguez Maranon, M. J., Mercier, D., van Huystee, R. B., and Stillman, M. J. (1994) Analysis of the optical absorption and magnetic-circular-dichroism spectra of peanut peroxidase: electronic structure of a peroxidase with biochemical properties similar to those of horseradish peroxidase, *Biochem. J. 301 (Pt 2)*, 335-341.
36. Volkov, A. N., Nicholls, P., and Worrall, J. A. R. (2011) The complex of cytochrome c and cytochrome c peroxidase: The end of the road?, *Biochim. Biophys. Acta. 1807*, 1482-1503.
37. Lawrence, A., Jones, C. M., Wardman, P., and Burkitt, M. J. (2003) Evidence for the role of a peroxidase compound I-type intermediate in the oxidation of glutathione, NADH, ascorbate, and dichlorofluorescin by cytochrome c/H2O2 - Implications for oxidative stress during apoptosis, *J. Biol. Chem. 278*, 29410-29419.
38. Florence, T. M. (1985) The Degradation of Cytochrome *c* by Hydrogen Peroxide, *J. Inorg. Biochem. 23*, 131-141.
39. Villegas, J. A., Mauk, A. G., and Vazquez-Duhalt, R. (2000) A cytochrome c variant resistant to heme degradation by hydrogen peroxide, *Chem. Biol. 7*, 237-244.
40. Gray, H. B., and Winkler, J. R. (2015) Hole hopping through tyrosine/tryptophan chains protects proteins from oxidative damage, *Proc. Natl. Acad. Sci. U.S.A. 112*, 10920-10925.
41. Barayeu, U., Lange, M., Mendez, L., Arnhold, J., Shadyro, O. I., Fedorova, M., and Flemmig, J. (2019) Cytochrome c autocatalyzed carbonylation in the presence of hydrogen peroxide and cardiolipins, *J. Biol. Chem. 294*, 1816-1830.
42. Keck, R. G. (1996) The use of t-butyl hydroperoxide as a probe for methionine oxidation in proteins, *Anal. Biochem. 236*, 56-62.
43. Shechter, Y., Burstein, Y., and Patchornik, A. (1975) Selective Oxidation of Methionine in Proteins, *Biochemistry 14*, 4497-4503.
44. Chen, Y.-R., Deterding, L. J., Sturgeon, B. E., Tomer, K. B., and Mason, R. P. (2002) Protein Oxidation of Cytochrome c by Reactive Halogen Species Enhances Its Peroxidase Activity, *J. Biol. Chem. 277*, 29781-29791.
45. Pande, J., Kinnally, K., Thallum, K. K., Verma, B. C., Myer, Y. P., Rechsteiner, L., and Bosshard, H. R. (1987) Methionine-oxidized horse heart cytochromes c. I. Reaction with Chloramine-T, products, and their oxidoreduction properties, *J. Protein Chem. 6*, 295-319.
46. Mushran, S. P., Agrawal, M. C., and Prasad, B. (1971) Mechanism of Oxidations by Chloramine-T .1. Oxidation of alpha-hydroxy-acids, *J. Chem. Soc. B 0*, 1712-1714.
47. Parakra, R. D., Kleffmann, G. N. L., Jameson, T., and Ledgerwood, E. C. (2018) The proportion of Met80-sulfoxide dictates peroxidase activity of human cytochrome c, *Dalton Trans. 47*, 9128-9135.
48. Campbell, M. M., and Johnson, G. (1978) Chloramine T and related N-halogeno-N-metallo reagents, *Chem. Rev. 78*, 65-79.
49. Lushington, G. H., Cowley, A. B., Silchenko, S., Lukat-Rodgers, G. S., Rodgers, K. R., and Benson, D. R. (2003) Comparison of Thioethers and Sulfoxides as Axial Ligands for N-Acetylmicroperoxidase-8: Implications for Oxidation of Methionine-80 in Cytochrome c, *Inorg. Chem. 42*, 7550-7559.

50. Wang, Z., Ando, Y., Nugraheni, A. D., Ren, C., Nagao, S., and Hirota, S. (2014) Self-oxidation of cytochrome c at methionine80 with molecular oxygen induced by cleavage of the Met-heme iron bond, *Mol. Biosyst. 10*, 3130-3137.
51. Birk, A. V., Chao, W. M., Liu, S. Y., Soong, Y., and Szeto, H. H. (2015) Disruption of cytochrome c heme coordination is responsible for mitochondrial injury during ischemia, *Biochim. Biophys. Acta 1847*, 1075-1084.
52. Nugraheni, A. D., Ren, C. G., Matsumoto, Y., Nagao, S., Yamanaka, M., and Hirota, S. (2018) Oxidative modification of methionine80 in cytochrome c by reaction with peroxides, *J. Inorg. Biochem. 182*, 200-207.
53. Diaz-Quintana, A., Perez-Mejias, G., Guerra-Castellano, A., De la Rosa, M. A., and Diaz-Moreno, I. (2020) Wheel and Deal in the Mitochondrial Inner Membranes: The Tale of Cytochrome c and Cardiolipin, *Oxidative Med. Cell. Longev. 2020*, 1-20.
54. Alvarez-Paggi, D., Hannibal, L., Castro, M. A., Oviedo-Rouco, S., Demicheli, V., Tórtora, V., Tomasina, F., Radi, R., and Murgida, D. H. (2017) Multifunctional Cytochrome c: Learning New Tricks from an Old Dog, *Chem. Rev. 117*, 13382-13460.
55. McClelland, L. J., Mou, T.-C., Jeakins-Cooley, M. E., Sprang, S. R., and Bowler, B. E. (2014) Structure of a mitochondrial cytochrome c conformer competent for peroxidase activity, *Proc. Natl. Acad. Sci. U.S.A. 111*, 6648-6653.
56. Kitt, J. P., Bryce, D. A., Minteer, S. D., and Harris, J. M. (2017) Raman Spectroscopy Reveals Selective Interactions of Cytochrome c with Cardiolipin That Correlate with Membrane Permeability, *J. Am. Chem. Soc. 139*, 3851−3860.
57. Oemer, G., Lackner, K., Muigg, K., Krumschnabel, G., Watschinger, K., Sailer, S., Lindner, H., Gnaiger, E., Wortmann, S. B., Werner, E. R., Zschocke, J., and Keller, M. A. (2018) Molecular structural diversity of mitochondrial cardiolipins, *Proc. Natl. Acad. Sci. U.S.A. 115*, 4158-4163.
58. Belikova, N. A., Vladimirov, Y. A., Osipov, A. N., Kapralov, A. A., Tyurin, V. A., Potapovich, M. V., Basova, L. V., Peterson, J., Kurnikov, I. V., and Kagan, V. E. (2006) Peroxidase Activity and Structural Transitions of Cytochrome c Bound to Cardiolipin-Containing Membranes, *Biochemistry 45*, 4998-5009.
59. Hersleth, H.-P., Ryde, U., Rydberg, P., Görbitz, C. H., and Andersson, K. K. (2006) Structures of the high-valent metal-ion haem–oxygen intermediates in peroxidases, oxygenases and catalases, *J. Inorg. Biochem. 100*, 460-476.
60. Bushnell, G. W., Louie, G. V., and Brayer, G. D. (1990) High-resolution Three-dimensional Structure of Horse Heart Cytochrome c, *J. Mol. Biol. 214*, 585-595.
61. Zinnel, N. F., Pai, P.-J., and Russell, D. H. (2012) Ion Mobility-Mass Spectrometry (IM-MS) for Top-Down Proteomics: Increased Dynamic Range Affords Increased Sequence Coverage, *Anal. Chem. 84*, 3390-3397.
62. Polasky, D. A., Lermyte, F., Nshanian, M., Sobott, F., Andrews, P. C., Loo, J. A., and Ruotolo, B. T. (2018) Fixed-Charge Trimethyl Pyrilium Modification for Enabling Enhanced Top-Down Mass Spectrometry Sequencing of Intact Protein Complexes, *Anal. Chem. 90*, 2756-2764.
63. Halgand, F., Habchi, J., Cravello, L., Martinho, M., Guigliarelli, B., and Longhi, S. (2011) Dividing To Unveil Protein Microheterogeneities: Traveling Wave Ion Mobility Study, *Anal. Chem. 83*, 7306-7315.
64. He, F., Hendricksen, C. L., and Marshall, A. G. (2000) Unequivocal Determination of Metal Atom Oxidation State in Naked Heme Proteins: Fe(III)Myoglobin,

Fe(III)Cytochrome c, Fe(III)Cytochrome b5, and Fe(III) Cytochrome b5 L47R, *J. Am. Soc. Mass Spectrom. 11*, 120-126.
65. Mark, K. J., and Douglas, D. J. (2006) Coulomb effects in binding of heme in gas-phase ions of myoglobin, *Rapid Commun. Mass Spectrom. 20*, 111-117.
66. Fisher, W. R., Taniuchi, H., and Anfinsen, C. B. (1973) On the Role of Heme in the Formation of the Structure of Cytochrome c, *J. Biol. Chem. 248*, 3188-3195.
67. Daltrop, O., and Ferguson, S. J. (2003) Cytochrome c maturation - The in vitro reactions of horse heart apocytochrome c and Paracoccus denitrificans apocytochrome c(550) with heme, *J. Biol. Chem. 278*, 4404-4409.
68. Capdevila, D. A., Marmisolle, W. A., Tomasina, F., Demicheli, V., Portela, M., Radi, R., and Murgida, D. H. (2015) Specific methionine oxidation of cytochrome c in complexes with zwitterionic lipids by hydrogen peroxide: potential implications for apoptosis, *Chem. Sci. 6*, 705-713.
69. Yin, V., Mian, S. H., and Konermann, L. (2019) Lysine carbonylation is a previously unrecognized contributor to peroxidase activation of cytochrome c by chloramine-T, *Chem. Sci. 10*, 2349-2359.
70. Mendoza, V. L., and Vachet, R. W. (2009) Probing Protein Structure by Amino Acid-specific Covalent Labeling and Mass Spectrometry, *Mass Spectrom. Rev. 28*, 785-815.
71. Jumper, C. C., and Schriemer, D. C. (2011) Mass Spectrometry of Laser-Initiated Carbene Reactions for Protein Topographic Analysis, *Anal. Chem. 83*, 2913–2920.
72. Shechter, Y., Burstein, Y., and Patchornik, A. (1975) Selective Oxidation of Methionine Residues in Proteins, *Biochemistry 14*, 4497-4503.
73. Michel, B., Proudfoot, A. E. I., Wallace, C. J. A., and Bosshard, H. R. (1989) The Cytochrome c Oxidase-Cytochrome c Complex: Spectroscopic Analysis of Conformational Changes in the Protein-Protein Interaction Domain, *Biochemistry 28*, 456-462.
74. Mirzaei, H., and Regnier, F. (2006) Identification and quantification of protein carbonylation using light and heavy isotope labeled Girard's P reagent, *J. Chromatogr. A 1134*, 122-133.
75. Santa, T. (2011) Derivatization reagents in liquid chromatography/electrospray ionization tandem mass spectrometry, *Biomed. Chromatogr. 25*, 1-10.
76. Li, Y. M., Polozova, A., Gruia, F., and Feng, J. H. (2014) Characterization of the Degradation Products of a Color-Changed Monoclonal Antibody: Tryptophan-Derived Chromophores, *Anal. Chem. 86*, 6850-6857.
77. Osman, A. M., Koerts, J., Boersma, M. G., Boeren, S., Veeger, C., and Rietjens, I. (1996) Microperoxidase/H2O2-catalyzed aromatic hydroxylation proceeds by a cytochrome-P-450-type oxygen-transfer reaction mechanism, *Eur. J. Biochem. 240*, 232-238.
78. Spector, A., Zhou, W., Ma, W. C., Chignell, C. F., and Reszka, K. J. (2000) Investigation of the mechanism of action of microperoxidase-11, (MP11), a potential anti-cataract agent, with hydrogen peroxide and ascorbate, *Exp. Eye Res. 71*, 183-194.
79. Konermann, L., Metwally, H., Duez, Q., and Peters, I. (2019) Charging and Supercharging of Proteins for Mass Spectrometry: Recent Insights into the Mechanisms of Electrospray Ionization, *Analyst 144*, 6157-6171.
80. Assfalg, M., Bertini, I., Dolfi, A., Turano, P., Mauk, A. G., Rosell, F. I., and Gray, H. B. (2003) Structural Model for an Alkaline Form of Ferricytochrome c, *J. Am. Chem. Soc. 125*, 2913-2922.

81. Garcia-Heredia, J. M., Diaz-Quintana, A., Salzano, M., Orzaez, M., Perez-Paya, E., Teixeira, M., De la Rosa, M. A., and Diaz-Moreno, I. (2011) Tyrosine phosphorylation turns alkaline transition into a biologically relevant process and makes human cytochrome c behave as an anti-apoptotic switch, *J. Biol. Inorg. Chem. 16*, 1155-1168.
82. Amacher, J. F., Zhong, F. F., Lisi, G. P., Zhu, M. Q., Alden, S. L., Hoke, K. R., Madden, D. R., and Pletneva, E. V. (2015) A Compact Structure of Cytochrome c Trapped in a Lysine-Ligated State: Loop Refolding and Functional Implications of a Conformational Switch, *J. Am. Chem. Soc. 137*, 8435-8449.
83. Gu, J., Shin, D.-W., and Pletneva, E. V. (2017) Remote Perturbations in Tertiary Contacts Trigger Ligation of Lysine to the Heme Iron in Cytochrome c, *Biochemistry 56*, 2950−2966.
84. Nakahara, K., Kitazawa, C., and Mineno, T. (2017) Chloramine-T-Mediated Oxidation of Benzylic Alcohols Using Indium(III) Triflate, *Chem. Pharm. Bull. 65*, 801-804.
85. Schaffner, I., Hofbauer, S., Krutzler, M., Pirker, K. a. F., Furtmüller, P. G., and Obinger, C. (2015) Mechanism of chlorite degradation to chloride and dioxygen by the enzyme chlorite dismutase, *Arch. Biochem. Biophys. 574*, 18-26.
86. Mashino, T., and Fridovich, I. (1988) Reactions of hypochlorite with catalase, *Biochim. Biophys. Acta 956*, 63-69.
87. Maitra, D., Byun, J., Andreana, P. R., Abdulhamid, I., Diamond, M. P., Saed, G. M., Pennathur, S., and Abu-Soud, H. M. (2011) Reaction of hemoglobin with HOCl: Mechanism of heme destruction and free iron release, *Free Radical Biol. Med. 51*, 374-386.
88. Hu, W. B., Kan, Z. Y., Mayne, L., and Englander, S. W. (2016) Cytochrome c folds through foldon-dependent native-like intermediates in an ordered pathway, *Proc. Natl. Acad. Sci. U.S.A. 113*, 3809-3814.
89. Maity, H., Rumbley, J. N., and Englander, S. W. (2006) Functional role of a protein foldon - An Omega-Loop foldon controls the alkaline transition in ferricytochrome c, *Proteins 63*, 349-355.
90. Deacon, O. M., Svistunenko, D. A., Moore, G. R., Wilson, M. T., and Worrall, J. A. R. (2018) Naturally Occurring Disease-Related Mutations in the 40-57 Omega-Loop of Human Cytochrome c Control Triggering of the Alkaline Isomerization, *Biochemistry 57*, 4276-4288.
91. Tomášková, N., Varhač, R., Lysáková, V., Musatov, A., and Sedlák, E. (2018) Peroxidase activity of cytochrome c in its compact state depends on dynamics of the heme region, *Biochim. Biophys. Acta 1866*, 1073–1083.
92. Requena, J. R., Chao, C.-C., Levine, R. L., and Stadtman, E. R. (2001) Glutamic and aminoadipic semialdehydes are the main carbonyl products of metal-catalyzed oxidation of proteins, *Proc. Natl. Acad. Sci. U.S.A. 98*, 69-74.
93. Chen, B. F., Brown, K. A., Lin, Z. Q., and Ge, Y. (2018) Top-Down Proteomics: Ready for Prime Time?, *Analytical Chemistry 90*, 110-127.
94. Crittenden, C. M., Novelli, E. T., Mehaffey, M. R., Xu, G. N., Giles, D. H., Fies, W. A., Dalby, K. N., Webb, L. J., and Brodbelt, J. S. (2020) Structural Evaluation of Protein/Metal Complexes via Native Electrospray Ultraviolet Photodissociation Mass Spectrometry, *J. Am. Soc. Mass Spectrom. 31*, 1140-1150.
95. Gomes, F. P., Diedrich, J. K., Saviola, A. J., Memili, E., Moura, A. A., and Yates, J. R. (2020) EThcD and 213 nm UVPD for Top-Down Analysis of Bovine Seminal Plasma

Proteoforms on Electrophoretic and Chromatographic Time Frames, *Anal. Chem. 92*, 2979-2987.

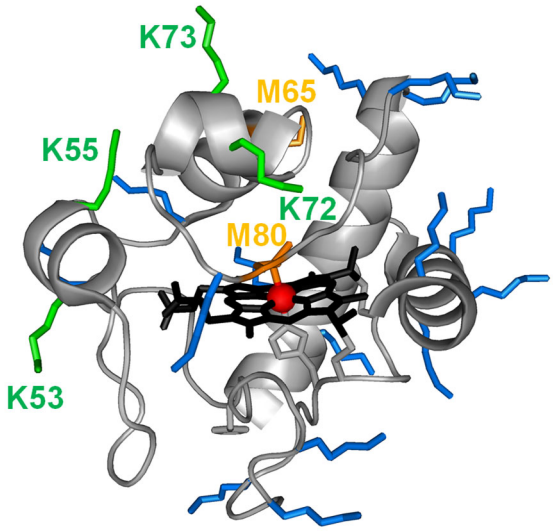

Figure 1. Crystal structure of equine holo-cyt *c* (PDB 1HRC).[60] Met residues are depicted in orange. Sites of LysCHO formation are depicted in green. All remaining Lys are depicted in blue. Heme is depicted in black, and the heme iron is shown in red.

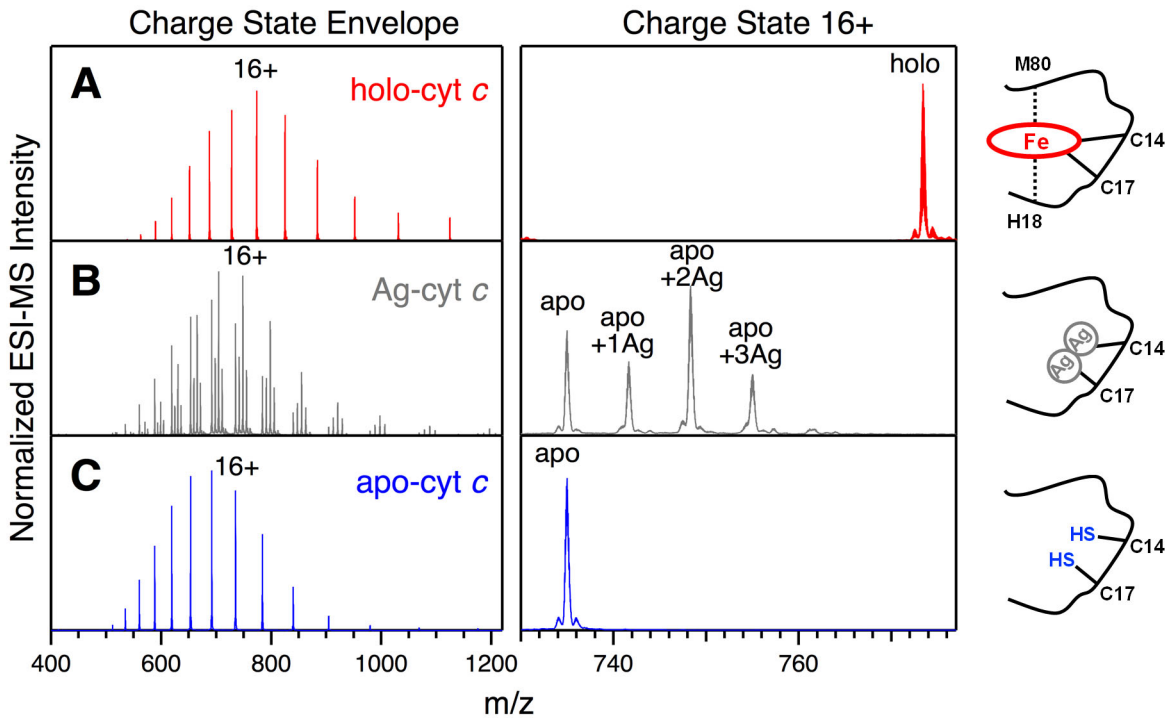

Figure 2. Left: Intact protein ESI mass spectra of different cyt *c* forms. (A) Holo-cyt *c* (unmodified control), (B) Ag-cyt *c*, (C) apo-cyt *c*. Far right: Cartoon representation of each form.

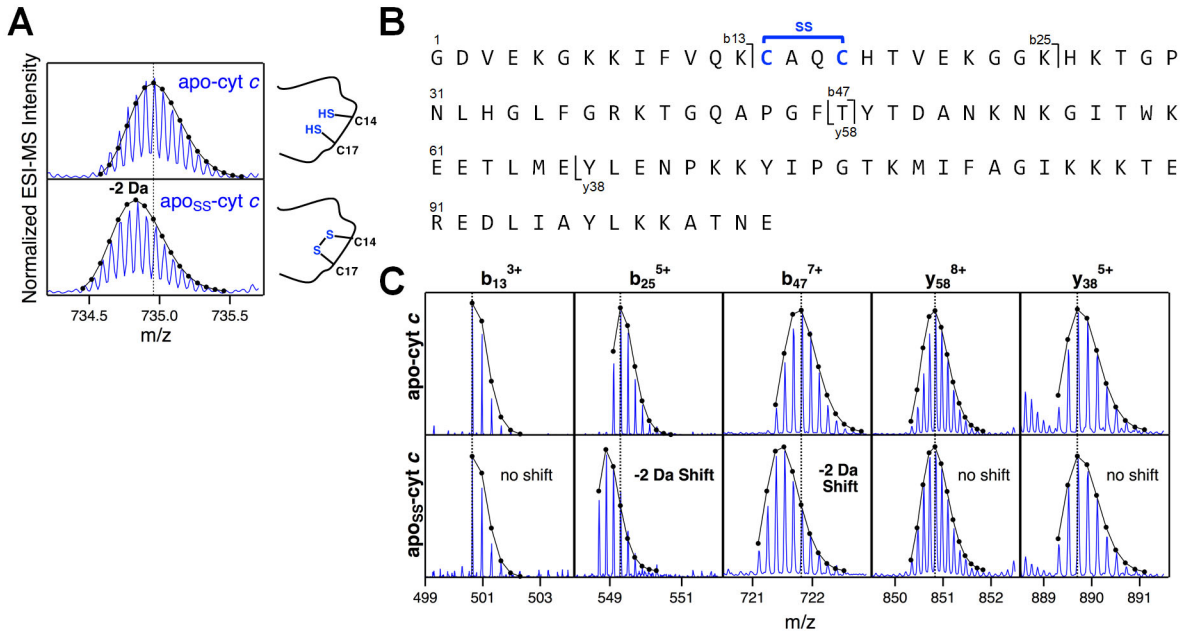

Figure 3. (A) Mass spectra of apo-cyt *c* highlighting a disulfide-induced mass shift after storage. (B) Aposs-cyt *c* sequence; selected top-down fragmentation sites are indicated. (C) Representative top-down CID-IM-MS fragment ions from apo-cyt *c* (top) and aposs-cyt *c* (bottom). All spectra are overlaid with their modeled isotope distributions (black dots and lines).

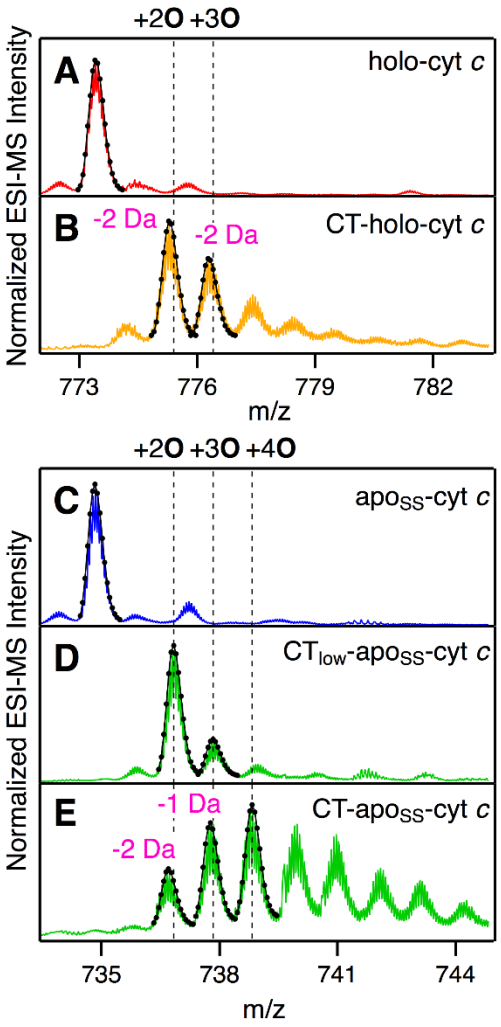

Figure 4. Intact protein mass spectra (charge state 16+) depicting the effects of cyt *c* oxidation by CT. (A) holo-cyt *c* (untreated control). (B) CT-holo-cyt *c*. (C) apoSS-cyt *c*. (D) CT_{low}-apoSS-cyt *c*. (E) CT-apoSS-cyt *c*. Black solid lines and dots are modeled isotope envelopes. Vertical dashed lines mark the positions expected for "clean" +*n*O modifications; experimentally observed deviations from these "clean" positions are indicated in pink.

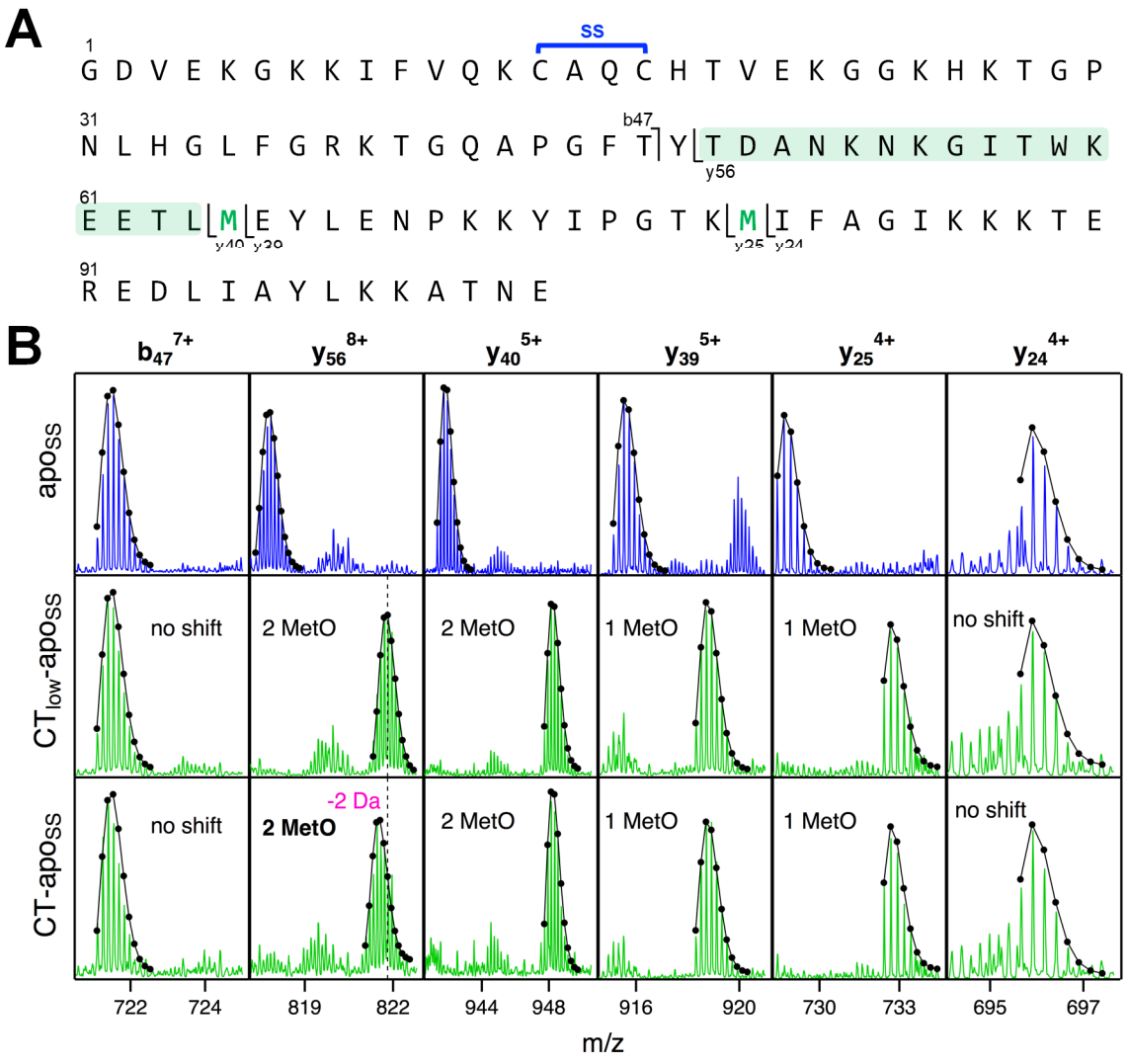

Figure 5. Top-down CID-IM-MS analysis of CT-apoSS-cyt *c*. (A) protein sequence with selected fragmentation sites. The remaining three panels show partial fragment spectra. The two modified Met residues are highlighted in color, along with the sequence range that harbors an additional -2 Da modification. (B) Top: apoSS-cyt *c* (untreated control). Center: CT_{low}-apoSS-cyt *c*. Bottom: CT-apoSS-cyt *c*. Each spectrum is overlaid with its theoretical isotopic envelope.

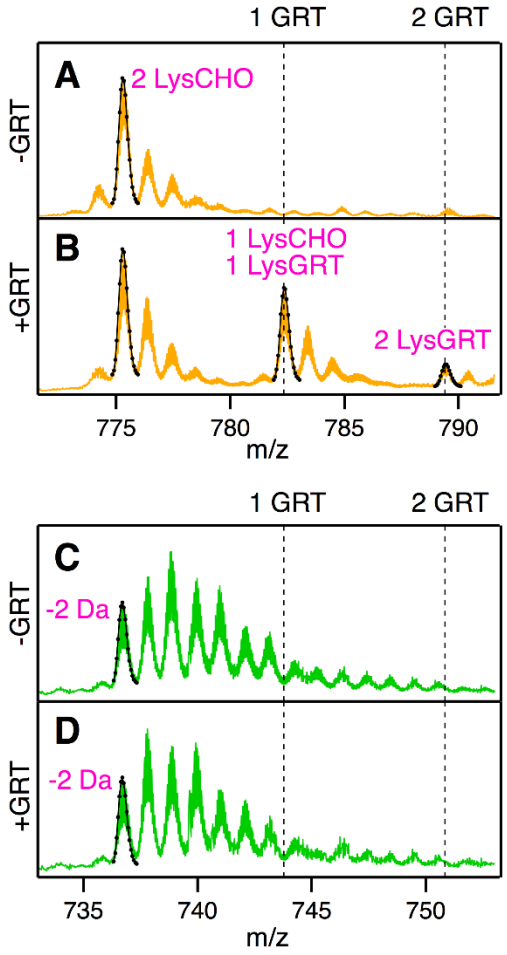

Figure 6. Intact protein mass spectra (charge state 16+) depicting the effects of GRT labeling. (A) CT-holo-cyt *c* prior to GRT labeling. (B) CT-holo-cyt *c* after GRT labeling. (C) CT-aposs-cyt *c* prior to GRT labeling (D) CT-aposs-cyt *c* after GRT labeling. Dashed vertical lines mark expected position of GRT-modified species. The first peak of each distribution is overlaid with its theoretical isotopic envelope.

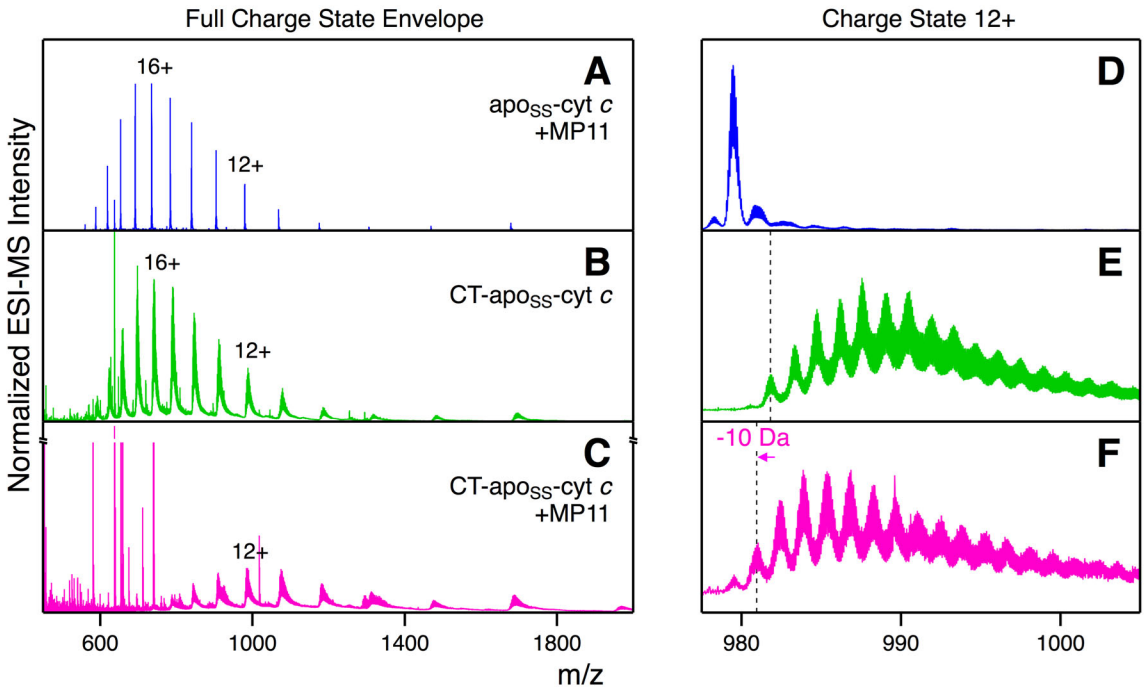

Figure 7. Intact protein mass spectra, illustrating the effects of MP11 during preparation of CT-aposs-cyt *c*. (A/D) aposs-cyt *c* with MP11 but without CT; (B/E) with CT but without MP11; (C/F) with CT and with MP11. (A-C) depict full charge state envelopes. (D-F) show a magnified view of the 12+ charge state. Vertical lines are present as a visual aid.

For Table of Contents use only